

## ELECTRON BREMSSTRAHLUNG HARD X-RAY SPECTRA, ELECTRON DISTRIBUTIONS, AND ENERGETICS IN THE 2002 JULY 23 SOLAR FLARE

GORDON D. HOLMAN,<sup>1</sup> LINHUI SUI,<sup>1,2</sup> RICHARD A. SCHWARTZ,<sup>1,3</sup> AND A. GORDON EMSLIE<sup>4</sup>

Received 2003 March 21; accepted 2003 July 17; published 2003 September 8

### ABSTRACT

We present and analyze the first high-resolution hard X-ray spectra from a solar flare observed in both X-ray/ $\gamma$ -ray continuum and  $\gamma$ -ray lines. Spatially integrated photon flux spectra obtained by the *Ramaty High Energy Solar Spectroscopic Imager (RHESSI)* are well fitted between 10 and 300 keV by the combination of an isothermal component and a double power law. The flare plasma temperature peaks at 40 MK around the time of peak hard X-ray emission and remains above 20 MK 37 minutes later. We derive the nonthermal mean electron flux distribution in one time interval by directly fitting the *RHESSI* X-ray spectrum with the thin-target bremsstrahlung from a double-power-law electron distribution with a low-energy cutoff. We find that relativistic effects significantly impact the bremsstrahlung spectrum above 100 keV and, therefore, the deduced mean electron flux distribution. We derive the evolution of the injected electron flux distribution on the assumption that the emission is thick-target bremsstrahlung. The injected nonthermal electrons are well described throughout the flare by a double-power-law distribution with a low-energy cutoff that is typically between 20 and 40 keV. We find that the power in nonthermal electrons peaks before the impulsive rise of the hard X-ray and  $\gamma$ -ray emissions. We compare the energy contained in the nonthermal electrons with the energy content of the thermal flare plasma observed by *RHESSI* and *GOES*. The minimum total energy deposited into the flare plasma by nonthermal electrons,  $2.6 \times 10^{31}$  ergs, is on the order of the energy in the thermal plasma.

*Subject headings:* Sun: flares — Sun: X-rays, gamma rays

The time history of the flare emission in three energy bands is shown in Figure 1a. The *Ramaty High Energy Solar Spectroscopic Imager (RHESSI)* uses two sets of aluminum attenuators, known as thin shutters and thick shutters, to avoid saturating the detectors during large flares. The July 23 flare was observed in two attenuator states. The instrument was primarily in the A3 state, with both sets of attenuators in place. Early in the flare, before 00:26:08 UT, and late in the flare, after 00:59:21 UT, the instrument was in the A1 state, with only the thin shutters in place. There were also four brief periods during which the instrument switched from A3 to A1 and back to A3. These transitions in attenuator state are apparent in the time history of the lowest energy band in Figure 1a. The flux calibration is currently uncertain during these four brief periods, so these time periods appear as gaps in subsequent results derived from the data.

We corrected the observed counts for pulse pileup and decimation (see Smith et al. 2002). Pulse pileup occurs at high count rates, with multiple photons recorded as a single photon with an energy equal to the sum of the energies of the individual photons. Decimation conserves onboard memory by recording only a fraction of the incident photons. Background counts were determined from the data by linearly interpolating between the background levels before and after the flare.

We obtained spectral fits using a forward fitting procedure, for which we assume the spectral form of the incident flux. We used an isothermal bremsstrahlung spectrum plus a double power law, giving us six free parameters. This function is folded through the instrument response for each attenuator state to

provide the expected count rates. The free parameters are varied until a minimum  $\chi^2$  fit to the count rates is obtained.

Spectra obtained in the A1 state were fitted down to 10 keV photon energies, while spectra obtained in the A3 state were fitted down to 15 keV. The attenuators substantially diminish the photon flux that reaches the *RHESSI* detectors at lower energies, and the calibration is currently not well established at these energies. The spectra were fitted up to 300 keV when possible. (The spectra above 300 keV are discussed in Share et al. 2003 and Smith et al. 2003.) At times earlier than 00:26:00 UT, for example, spectral fits could not be obtained above 60 keV. We estimate the systematic uncertainty in the fluxes in each energy bin, which dominates the random (Poisson) noise at high count rates, to be 2% in the A3 state and 5% in the A1 state. These estimates were obtained by requiring the reduced  $\chi^2$  for our spectral fits to be  $\sim 1$ .

During the early rise of the flare, before 00:26:20 UT, we found that the spectra could be fitted with a double power law alone. An equally good fit could be obtained with the combination of an isothermal component and a double power law above  $\sim 18$  keV. The results of this fit are shown in Figure 1. Late in the flare, only the isothermal component is evident.

The temperature rapidly rises to “superhot” values (Lin et al. 1981) as high as 40 MK. This hot thermal emission is consistent with the spectrum of the “coronal” source observed in *RHESSI* images (Emslie et al. 2003), although our derived temperatures are somewhat lower. The plasma gradually cools after the end of the first peak in the flare emission, with some reheating in subsequent peaks. The plasma temperature derived from the *RHESSI* spectra remains above 20 MK for at least 37 minutes after reaching its peak value. Temperatures derived from *GOES* data are shown for comparison (Fig. 1b, *solid curve*). Throughout the flare, the temperatures derived from the *RHESSI* data are typically around 10 MK higher than those derived from *GOES*. These higher temperatures are expected for a multithermal plasma, since *RHESSI* is sensitive to higher photon energies than

<sup>1</sup> Laboratory for Astronomy and Solar Physics, Code 682, NASA Goddard Space Flight Center, Greenbelt, MD 20771; holman@stars.gsfc.nasa.gov, lhsui@stars.gsfc.nasa.gov, richard.schwartz@gsfc.nasa.gov.

<sup>2</sup> Department of Physics, Catholic University of America, 620 Michigan Avenue, Washington, DC 20064.

<sup>3</sup> Science Systems and Applications, Inc., Aerospace Building, 10210 Greenbelt Road, Suite 500, Lanham, MD 20706.

<sup>4</sup> Department of Physics, The University of Alabama in Huntsville, Huntsville, AL 35899; emslie@uah.edu.

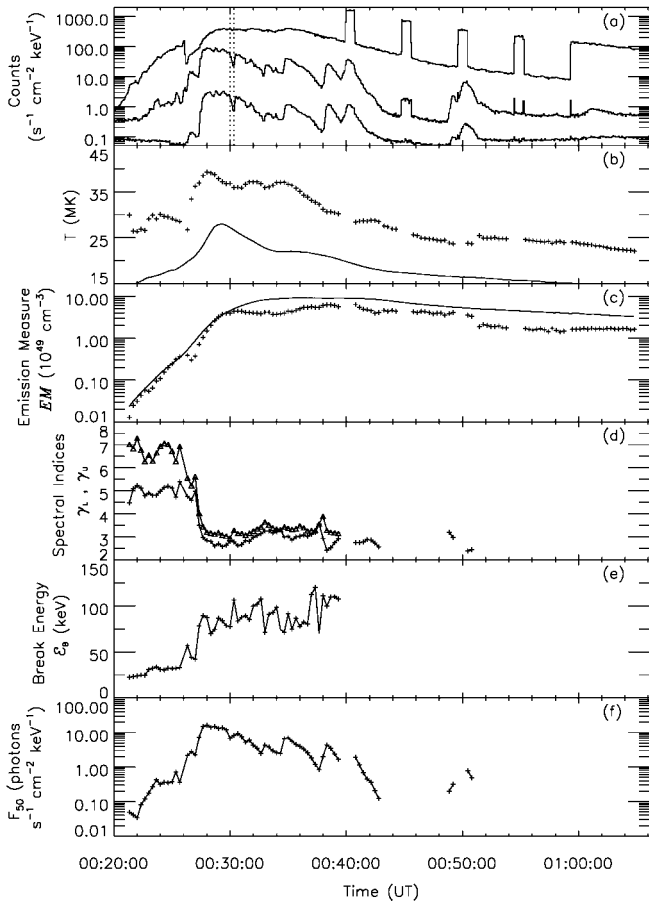


FIG. 1.—*RHESSI* X-ray light curves and time history of fit parameters. (a) Light curves in three energy bands, scaled to avoid overlap. The energy bands and scale factors are 12–40 (*top curve*,  $\times 0.6$ ), 40–100 (*middle curve*,  $\times 3$ ), and 100–300 keV (*bottom curve*,  $\times 1$ ). The dotted vertical lines show the beginning and end of the integration time interval for the spectrum in Fig. 2. (b) Temperature of the isothermal component (20 s time resolution; *plus signs*). The solid curve is the temperature derived from *GOES* data. (c) Isothermal emission measure (*plus signs*). The solid curve is the emission measure derived from *GOES* data, scaled by a factor of 0.25. (d) Spectral indices (spectral index below break, *plus signs*; spectral index above break, *triangles*). (e) Break energy in the double-power-law spectra. (f) Photon flux at 50 keV, determined from the double-power-law fit.

*GOES*. Although the peak temperature is similar to that obtained by Lin et al. (1981) for the 1980 June 27 flare, the peak emission measure is 30 times greater, consistent with the higher X-ray intensity of this flare. The *GOES* emission measure (*solid curve*; scaled by a factor of 0.25) always exceeds the *RHESSI* result, as expected for the lower temperatures obtained from *GOES*.

The spectral indices  $\gamma_L$  and  $\gamma_U$ , defined by flux proportional to  $\mathcal{E}^{-\gamma}$ , have values between 2.5 and 3.5 after the impulsive rise of the flare. These spectral indices and their time evolution are consistent with the spectra obtained for the “footpoint” sources observed in *RHESSI* images (Emslie et al. 2003). Earlier in the flare, before the impulsive rise at 00:27:00 UT, the indices are much greater. The break energy increases from values below 50 keV before the impulsive rise of the flare to values in the range 70–125 keV afterward. When the non-thermal spectrum is observable after 00:40:00 UT, it is best fitted with a single power law.

We deduce the electron flux distributions by assuming that their functional form is a double power law (power-law index  $\delta_L$  below a break energy  $E_B$ ,  $\delta_U$  above) with a low-energy cutoff

( $E_c$ ). We fitted the observed count rate spectra with an isothermal bremsstrahlung component and the bremsstrahlung spectrum computed from this double-power-law distribution, using the same forward fitting technique described above. This gives a seven parameter fit. Our computations use the relativistic bremsstrahlung cross section of Haug (1997) with the Elwert (1939) correction.

We first compute the mean electron flux distribution for the time interval 00:30:00–00:30:20 UT (see Fig. 1a) and the 15–300 keV photon energy range, for comparison with the results of Piana et al. (2003) and Kontar et al. (2003). Piana et al. derive the mean electron flux distribution for this same time interval using a regularized, direct inversion procedure, while Kontar et al. include nonuniform target ionization in their spectral fit. The mean electron flux distribution (in units of electrons  $\text{cm}^{-2} \text{s}^{-1} \text{keV}^{-1}$ ) is the spatially averaged value of the electron flux weighted by the plasma density (Brown, Emslie, & Kontar 2003). This distribution is independent of any assumptions regarding the evolution of electrons in the source and, therefore, is well suited for comparison with electron distributions computed from theoretical flare models. Deducing the mean electron flux from a photon spectrum is equivalent to deducing the electron flux under the assumption that the radiation is thin-target bremsstrahlung from a spatially homogeneous electron flux distribution.

The result of our fit is shown in the top panel of Figure 2. The best-fit parameters are provided in the figure caption. Plotted in the middle panel are the residuals from this fit, defined as  $[F_{\text{obs}}(\mathcal{E}) - F_{\text{fit}}(\mathcal{E})]/\sigma(\mathcal{E})$ , where  $\mathcal{E}$  is the photon energy,  $F_{\text{obs}}$  is the observed photon flux,  $F_{\text{fit}}$  is the photon flux given by the model at energy  $\mathcal{E}$ , and  $\sigma$  is the uncertainty in the observed flux. The uncertainty  $\sigma$  includes both the systematic uncertainty, discussed above, and the Poisson statistics, added in quadrature. The residuals are limited to about the  $\pm 2 \sigma$  level. In the bottom panel, the mean electron flux distribution is plotted as a function of electron energy. The fit to the photon flux spectrum actually provides the quantity  $\bar{n}V\bar{F}(E)$ , where  $V$  is the volume of the emitting region,  $\bar{n}$  is the mean density of the thermal plasma in the emitting volume, and  $\bar{F}(E)$  is the mean electron flux distribution, so this is what is plotted. In the third fit parameter,  $\bar{F}$  is the mean electron flux distribution integrated from  $E_c$  to the highest electron energy in the distribution (we used a value of 5 MeV).

The break energy,  $E_B$ , for the electron distribution is higher than that for the photon spectrum ( $E_B = 77$  keV) because bremsstrahlung photons are produced by electrons with higher energies than the photon energy. The photon spectrum below  $E_c$  flattens to about  $\mathcal{E}^{-1}$ . The power-law indices  $\delta_L = 1.5$  and  $\delta_U = 2.5$  for the mean electron flux distribution are smaller than the photon spectral indices  $\gamma_L = 2.8$  and  $\gamma_U = 2.9$ , but not by 1 as predicted for nonrelativistic thin-target bremsstrahlung from a single-power-law electron flux distribution. For this relatively flat electron distribution, relativistic flattening of the bremsstrahlung spectrum is important at photon energies above 100 keV. Therefore,  $\delta_U$  is larger than 1.9 to compensate for the fact that the observed spectrum does not flatten above 100 keV. To prevent the photon spectrum from being too steep below 100 keV,  $\delta_L$  is somewhat less than 1.8.

The result of Piana et al. using the regularized direct inversion procedure is quite similar to ours but shows a dip in the mean electron flux distribution between 50 and 60 keV. Kontar et al. find that injection of the electrons into a nonuniformly ionized target plasma provides a better fit to the spectrum than a single-

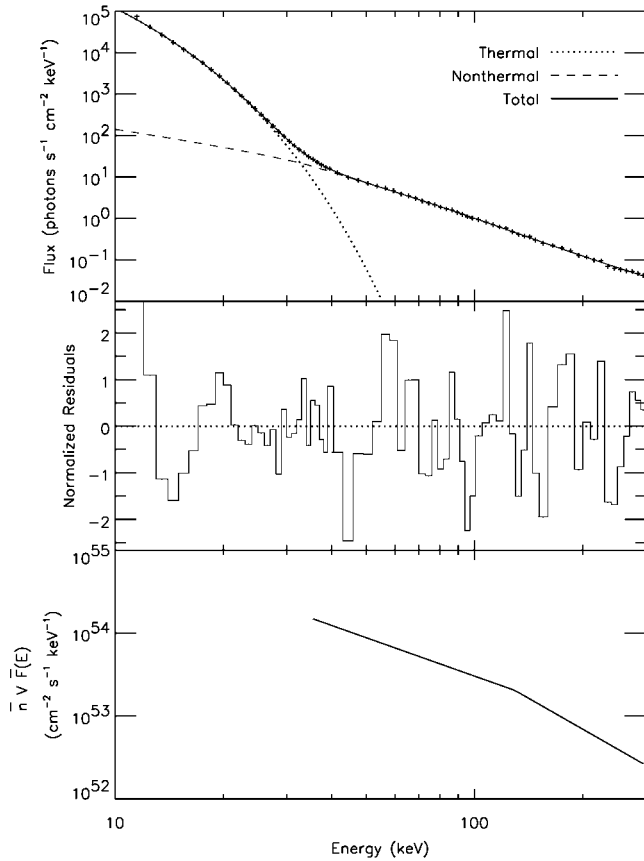


FIG. 2.—Mean electron flux fit and residuals for the 00:30:00–00:30:20 UT time interval. The fit to the photon flux (*plus signs*) in the top panel, plotted as a function of photon energy in units of keV, is the bremsstrahlung from an isothermal plasma (*dotted curve*) and a double-power-law mean electron flux distribution with a low-energy cutoff (*dashed curve*). The solid curve is the total fit. The best-fit parameters were  $EM = 4.1 \times 10^{49} \text{ cm}^{-3}$ ,  $T = 37 \text{ MK}$ ,  $\bar{n}v\bar{F} = 6.9 \times 10^{55} \text{ cm}^{-2} \text{ s}^{-1}$ ,  $E_c = 34 \text{ keV}$ ,  $\delta_L = 1.5$ ,  $E_B = 129 \text{ keV}$ , and  $\delta_U = 2.5$  with a reduced  $\chi^2$  of 0.94. The residuals in the middle panel are defined as the observed flux minus the model flux divided by the estimated  $1 \sigma$  uncertainty in each data point. The bottom panel shows the mean electron flux distribution times  $\bar{n}v$ , plotted as a function of electron energy in units of keV.

power-law distribution. All three distributions provide an acceptable  $\chi^2$  fit to the photon spectrum. The differences in these derived electron distributions highlight the fact that there is not a unique electron distribution associated with an observed count rate spectrum. The residuals of all three fits show some systematic variation with photon energy, especially below  $\sim 30 \text{ keV}$ . We are currently exploring whether these residuals contain enough information to distinguish the different fits.

We now derive the evolution of the injected electron flux distribution (in units of electrons  $\text{s}^{-1} \text{ keV}^{-1}$ ; Fig. 3) on the assumption that the nonthermal hard X-ray emission is thick-target bremsstrahlung (Brown 1971). The upper electron power-law indices (Fig. 3*b*, *triangles*) are larger by about 1 than the upper photon spectral indices, as expected ( $\delta_U \approx \gamma_U + 1$ ). (The relativistic flattening of the bremsstrahlung spectrum is not as prominent for thick-target emission as it is for thin-target emission.) The lower power-law indices are only slightly steeper than the lower photon indices, however, because fewer electrons are present above the break energy than would have been present for a single power law. The break energy (Fig. 3*c*) increases with time from values around 30 keV to values in excess of 200 keV. Before 00:23:20 UT and after

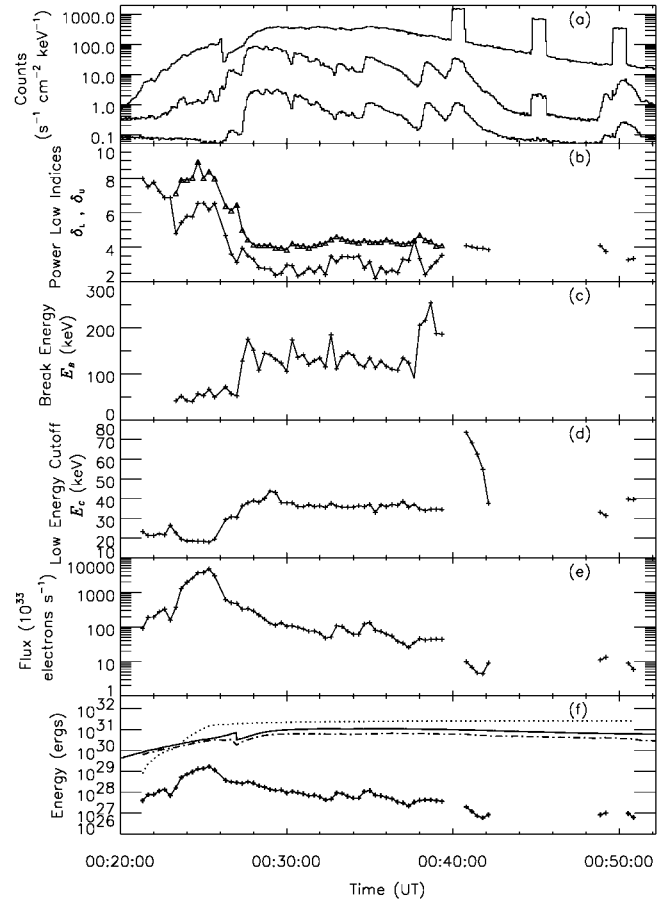


FIG. 3.—Thick-target bremsstrahlung electron flux distribution fit parameters and energetics. (a) X-ray light curves in three energy bands (see Fig. 1*a*). (b) Upper and lower power-law indices (20 s time resolution, same symbols as Fig. 1*d*). (c) Break energy in the double-power-law electron flux distribution. (d) Low-energy cutoff in the electron flux distribution. (e) Integrated (over all electron energies) electron flux. (f) Thermal and nonthermal energetics. The time history of the energy in the *GOES* (*solid line*) and *RHESSI* (*dot-dashed line*) isothermal fits is plotted using volumes estimated from *RHESSI* images (see text). This is compared to the accumulated energy in nonthermal electrons (*dotted curve*). The bottom curve, marked with plus signs, is the energy injection rate (in units of  $\text{ergs s}^{-1}$ ).

00:40:00 UT, the spectra were best fit with the isothermal component and a single power law with a low-energy cutoff. For most of the spectra after 00:40:00 UT, as with the photon fits, only the isothermal component was evident.

The low-energy cutoff (Fig. 3*d*) minimizes the energy in nonthermal electrons. Except for the brief period between 00:40:40 and 00:42:00 UT, when it was as high as 73 keV, the low-energy cutoff is near the photon energy at which the isothermal (exponential) photon spectrum flattens to the nonthermal power-law spectrum. We note that this location for the low-energy cutoff is comparable to that obtained with a hybrid thermal/nonthermal electron acceleration model in which the hot flare plasma and a tail of runaway electrons are produced simultaneously (Holman & Benka 1992; Benka & Holman 1994). The low-energy cutoff increases from around 20 keV before 00:26:00 UT to 30–40 keV after this time.

The distributions before 00:26:00 UT are also consistent with a double power law alone and no isothermal component. We could also fit them with a single power law with a high-energy cutoff (no isothermal component). The high-energy cutoff in-

creases from 40 keV at early times to as high as 100 keV at later times. However, we found that these spectra could not be adequately fitted with only a single power law with a low-energy cutoff (no isothermal component) or with an isothermal distribution alone.

The total electron flux, integrated over all electron energies, is plotted in Figure 3e. It reaches its maximum value of  $5 \times 10^{36}$  electrons  $s^{-1}$  at 00:25:20 UT. Note that this is before the impulsive rise after 00:27:00 UT and the appearance of the much harder X-ray spectra and the  $\gamma$ -ray line emission.

We can estimate the total density of nonthermal electrons by dividing the flux distribution function by the electron speed and the area of the thick-target interaction region and integrating over all electron energies. We first obtain a lower limit on the density at the time of peak electron flux by assuming that the entire source area is thick-target. Using the *RHESSI* image of White et al. (2003) at 00:24:57 UT (their Fig. 2c), we estimate an area of  $10^{19}$  cm<sup>2</sup>. This gives a density in suprathermal electrons of  $6 \times 10^7$  cm<sup>-3</sup> at 00:25:20 UT. The nonthermal source area later in the flare has been estimated by White et al. (2003) to be  $10^{17}$  cm<sup>2</sup>. This gives densities that are up to an order of magnitude higher. In interpreting their radio observations of the flare, White et al. deduce a nonthermal electron density of  $10^{11}$  cm<sup>-3</sup> above 10 keV at 00:35:00 UT. We obtain a density of  $3 \times 10^9$  cm<sup>-3</sup> at this time if the electron distribution extends down to 10 keV. Most of the difference in these densities can be attributed to the flattening of the electron distribution below the break energy of 134 keV in our fit. If we were to extrapolate the part of the electron distribution that is relevant to the optically thin radio observations, that above the break energy, down to 10 keV, the inferred density would be  $2.4 \times 10^{10}$  cm<sup>-3</sup>.

The energy flux (*solid curve with plus signs*) and the total accumulated energy deposited into the flare plasma (*dotted curve*) by electrons with energies above  $E_c$  are plotted as a function of time in Figure 3f. The energy flux (power) is obtained by multiplying the electron flux distribution derived for each 20 s interval times the electron energy and integrating over all energies above  $E_c$ . The accumulated energy is obtained by multiplying the energy flux at each time by the time interval (20 s) and obtaining the sum of these energies up to the time of interest. Note that about two-thirds of this energy is deposited before 00:26:00 UT. The total energy injected by these electrons during the whole flare is found to be  $2.6 \times 10^{31}$  ergs.

The energies ( $E_{th}$ ) contained in the thermal plasmas observed by *RHESSI* (*dot-dashed line*) and by *GOES* (*solid line*) are also plotted in Figure 3f. These curves are computed from  $E_{th} = 3nkTV = 3kT(EM \times V)^{1/2}$ , where the temperature ( $T$ ) and emission measure (EM) are obtained from the spectral fits. We estimate the volume ( $V$ ) of the thermal plasma from the *RHESSI* images. Before 00:27:00 UT we use the total source area in Figure 2c of White et al. (2003) to estimate the volume to be  $2 \times 10^{28}$  cm<sup>3</sup>. After 00:27:00 UT, during the main phase of the flare, we obtain  $4 \times 10^{27}$  cm<sup>3</sup> using the area of the coronal source in Figure 1 of Krucker et al. (2003). Since *GOES* did not provide images, we have no direct estimate of the volume of this plasma. Therefore, these same volumes are used to compute the energy

in the plasma observed by *GOES*. We can also estimate the density of the thermal plasma,  $n = (EM/V)^{1/2}$ . For an emission measure of  $5 \times 10^{49}$  cm<sup>-3</sup>, typical of the main phase of the flare (Fig. 1c), we obtain a density of  $1 \times 10^{11}$  cm<sup>-3</sup>.

We see from Figure 3f that even with the low-energy cutoffs derived here, the accumulated energy in the nonthermal electrons is comparable to the energy in the thermal plasma observed by both *RHESSI* and *GOES*. The peak energy in the thermal plasmas,  $6.6 \times 10^{30}$  ergs for *RHESSI* and  $1.1 \times 10^{31}$  ergs for *GOES*, is reached at about 00:36:00 UT. The energy deposited by the nonthermal electrons may be somewhat less than the energy in the thermal plasma if the volume of the plasma observed by *GOES* is at least  $\sim 4$  times greater than the volume of the hotter plasma observed by *RHESSI*. Otherwise, the energy is equal to or exceeds the thermal energy. Although we cannot determine from these results whether the energy contained in the nonthermal electrons was greater than or less than the energy in the hot thermal plasma, it is nevertheless significant that they are comparable, despite our spectral fits that minimize the energy in the nonthermal electrons.

Low-energy cutoffs lower than the values derived here are also consistent with the *RHESSI* spectra. Therefore, the energy deposited by the nonthermal electrons may be greater. Using our derived temperatures and the results of Emslie (2003), we find the maximum energy that the electrons could have injected into the flare plasma to be  $4 \times 10^{34}$  ergs. It is unlikely that the electrons deposited this much energy, since it is greater than the maximum total energy that has been deduced previously for even the largest solar flares.

The July 23 flare hard X-ray spectral data provide support for the longstanding impression that the energy in accelerated electrons is a major part of the energy released in many, if not all, flares. Our result for the energy injected by nonthermal electrons depends, however, on our nonthermal thick-target interpretation of the double-power-law fits. One compelling alternative is that the X-ray emission observed in the early rise phase of the flare (before 00:26:00 UT) is, at least in part, thin-target bremsstrahlung from the corona (Lin et al. 2003). The extended size of the X-ray source at this time is suggestive of this interpretation. However, this is likely to increase, rather than decrease, the total energy in nonthermal electrons. We note that if the flattening of the spectra below  $E_b$  is due to partial ionization in the target rather than a break in the electron distribution, the energy in nonthermal electrons increases. Another possibility is that the emission is from a multithermal plasma, but temperatures exceeding 100 MK would be required for this interpretation. A study of these alternatives is in progress.

This work was supported in part by the *RHESSI* Project and the NASA Sun-Earth Connection program. We thank Paul Bildeau, Sally House, and Kim Tolbert for their invaluable help with the *RHESSI* software. We thank Brian Dennis and the anonymous referee, whose comments and suggestions led to many improvements in this Letter. We also thank Hugh Hudson, Nichole Vilmer, and Stephen White for their helpful comments. This work would not have been possible without the dedicated efforts of the entire *RHESSI* team.

#### REFERENCES

- Benka, S. G., & Holman, G. D. 1994, *ApJ*, 435, 469  
 Brown, J. C. 1971, *Sol. Phys.*, 18, 489  
 Brown, J. C., Emslie, A. G., & Kontar, E. P. 2003, *ApJ*, 595, L115  
 Elwert, G. 1939, *Ann. Phys.*, 34, 178  
 Emslie, A. G. 2003, *ApJ*, 595, L119  
 Emslie, A. G., Kontar, E. P., Krucker, S., & Lin, R. P. 2003, *ApJ*, 595, L107  
 Haug, E. 1997, *A&A*, 326, 417  
 Holman, G. D., & Benka, S. G. 1992, *ApJ*, 400, L79

- Kontar, E. P., Brown, J. C., Emslie, A. G., Schwartz, R. A., Smith, D. M., & Alexander, R. C. 2003, ApJ, 595, L123
- Krucker, S., Hurford, G. J., & Lin, R. P. 2003, ApJ, 595, L103
- Lin, R. P., et al. 2003, ApJ, 595, L69
- Lin, R. P., Schwartz, R. A., Pelling, R. M., & Hurley, K. C. 1981, ApJ, 251, L109
- Piana, M., Massone, A. M., Kontar, E. P., Emslie, A. G., Brown, J. C., & Schwartz, R. A. 2003, ApJ, 595, L127
- Share, G., Murphy, R. J., Lin, R. P., Smith, D. M., & Schwartz, R. A. 2003, ApJ, 595, L89
- Smith, D. M., Share, G. H., Murphy, R. J., Schwartz, R. A., Shih, A. Y., & Lin, R. P. 2003, ApJ, 595, L81
- Smith, D. M., et al. 2002, Sol. Phys., 210, 33
- White, S. M., Krucker, S., Shibasaki, K., Yokoyama, T., Shimojo, M., & Kundu, M. R. 2003, ApJ, 595, L111